KSME International Journal, Vol. 16 No. 12, pp. 1561~1575, 2002

Control of Boundary Layer Flow Transition via Distributed Reduced-Order Controller

Keun Hyoung Lee*

Department of Mechanical & Aerospace Engineering, University of California, Los Angeles, California 90095, USA

A reduced-order linear feedback controller, which is used to control the linear disturbance in two-dimensional plane Poiseuille flow, is applied to a boundary layer flow for stability control. Using model reduction and linear-quadratic-Gaussian/loop-transfer-recovery control synthesis, a distributed controller is designed from the linearized two-dimensional Navier-Stokes equations. This reduced-order controller, requiring only the wall-shear information, is shown to effectively suppress the linear disturbance in boundary layer flow under the uncertainty of Reynolds number. The controller also suppresses the nonlinear disturbance in the boundary layer flow, which would lead to unstable flow regime without control. The flow is relaminarized in the long run. Other effects of the controller on the flow are also discussed.

Key Words: Robust, Optimal Control, Boundary Layer, Drag Reduction

Nomenclature

$\mathbf{A}, \mathbf{B}, \mathbf{C}, \mathbf{D}$: Matrices associated with state-space equation

$\hat{\mathbf{A}}, \hat{\mathbf{B}}, \hat{\mathbf{C}}, \mathbf{D}$: Matrices associated with reduced-order state-space equation

$\mathbf{A}_c$: Loop coefficient matrix

$\mathbf{A}_f$: Matrix associated with error evolution equation

A_m : Amplitude of disturbance

$a_{mn}, b_{mn}, c_{mn}, d_{mn}$: Coefficients of spectral decomposition

$\mathbf{e}_a$: Error between internal state $\hat{\mathbf{x}}_a$ and estimate state $\tilde{\mathbf{x}}_a$

$\mathbf{F}$: Matrix associated with cost criterion

g : Forcing term in Navier-Stokes equation

h : half channel height

$\mathbf{I}$: Identity matrix

$\hat{\mathbf{K}}_a$: Control gain matrix

L : 4^{th} order operator for linear term

L_x : Horizontal length

$\hat{\mathbf{L}}_a$: Kalman gain matrix

N : 4^{th} order operator for nonlinear term

$\mathbf{N}_a$: Matrix associated with cost criterion, $\hat{\mathbf{C}}_a^T \mathbf{D}_a$

P : Pressure

$\mathbf{P}_a$: Conditional error variance

$\mathbf{Q}_a$: Matrix associated with cost criterion, $\hat{\mathbf{C}}_a^T \hat{\mathbf{C}}_a$

$\mathbf{R}_a$: Matrix associated with cost criterion, $\mathbf{D}_a^T \mathbf{D}_a + \mathbf{F}_a^T \mathbf{F}_a$

Re : Real part of complex number

Re : Reynolds number based on half channel height

Re_{δ^*} : Reynolds number based on displacement thickness

$\mathbf{S}_a$: Solution of algebraic Riccati equation

t : time

U : Mean velocity in Poiseuille flow

U_B : Blasius mean velocity

$\mathbf{u}$: Input vector

u : Disturbance velocity

$\hat{u}(y)$: Eigenfunction of Orr-Sommerfeld solution

$\tilde{u}$: Intermediate velocity

v_w : Blowing/suction at wall

* **E-mail** : keun_99@yahoo. com
TEL : +1-310-825-0875;
Department of Mechanical & Aerospace Engineering, University of California, Los Angeles, California 90095, USA. (Manuscript **Received** March 2, 2001; **Revised** September 27, 2002)

$\mathbf{V}$, $\mathbf{W}$: Power spectral density of $\mathbf{v}$ and $\mathbf{w}$
$\mathbf{v}$, $\mathbf{w}$: White Gaussian noise associated with LQG
$\boldsymbol{x}$: State-space vector
$\hat{\boldsymbol{x}}$: Reduced-order state space vector
$\bar{\boldsymbol{x}}$: Conditional mean estimate of $\hat{\boldsymbol{x}}$
x, y : Physical coordinate
y_{max} : Height of physical domain of boundary layer flow
Z_t : Measurement history
$\mathbf{z}$: Output vector
z : Wall-shear measurement
α : Wavenumber
$\alpha_l, \beta_l, \gamma_l, \varsigma_l$: Coefficients associated with RK3
β, ρ : Tuning parameter for LQG/LTR
$\boldsymbol{\Gamma}_a$: Input matrix associated with LQG problem
Γ_m : Combination of Chebyshev polynomial
Δ : Laplacian operator
δ_* : Displacement thickness
$\delta_{i,1}$: Kronecker delta function
$\Im$: Cost criterion
ψ : Streamfunction
η_{max} : Height of computational domain of boundary layer flow
ϕ : Pseudo pressure
σ : Parameter to determine the grid concentration
ν : Kinematic viscosity
ν_a : Filter residual
ω : Eigenvalue of Orr-Sommerfeld solution

Superscript

n : Time step

Subscripts

i, j : Index representing horizontal and wall-normal direction (=1, 2)
n : Wavenumber index
l : RK substep (=1, 2, 3)

1. Introduction

Increasing attention has been given to the control of transitional flows in a variety range of structures such as nozzles, engine inlet/outlets, automobiles, submarines, airplanes over the last decade. Turbulent boundary layers have a high wall-shear stress compared to laminar flows. Therefore, a suppression or delay of transition can reduce the viscous drag acting on the surface of structures, leading to improve the efficiency of these configurations. Various methodologies and overviews on the control of flow were given by Gad-el-Hak (1989) and Gad-el-Hak and Bushnell (1991).

A variety of techniques and theories (Gad-el-Hak, 1989; 1994 Gad-el-Hak and Bushnell, 1991; Modi, 1997; Reed et al., 1996; Choi et al., 1993; 1994; Akhavan et al., 1993; Berger et al., 1997; Bewley and Moin, 1994; Lee et al., 1997; Koumoutsakos, 1999; Joshi et al., 1995; 1997; 1999; Bewley and Liu, 1998; Cortelezzi and Speyer, 1998; Cortelezzi et al., 1998; Lee et al., 2001; Lee, 1999; Lim and Kim, 2000) were attempted with partial success to control near-wall turbulence for drag reduction or transition delay. Over the past two decades, tools of designing distributed controller, which is thought to be more suitable in analyzing and controlling fluid flow, have been developed in the control/automation society (Zhou et al., 1996; Bryson and Ho, 1969; Kwakernaak and Silvan, 1969; Doyle and Stein, 1981; Rhee and Speyer, 1991). With the aid of these tools, a linear optimal controller was shown to reduce the viscous drag even in turbulent channel flows, (Lee et al., 2001; Lee, 1999) which is naturally nonlinear. The reason a linear controller works even in a turbulent flow was partially addressed by Kim and Lim (2000).

Multi-input/multi-output (MIMO) linear quadratic Gaussian (LQG) synthesis, or, in modern term $\boldsymbol{H}_2$ synthesis, combined with modern model reduction technique was used to design an optimal and robust linear controller for suppressing near-wall disturbances leading to transition in a two-dimensional laminar channel flow (Cortelezzi and Speyer, 1998).

The distributed robust linear controller based on two-dimensional linearized Navier-Stokes equations was shown to efficiently suppress finite near-wall disturbance in a two-dimensional channel (Cortelezzi et al., 1998) and near-wall turbu-

lence in a fully developed turbulent channel flow. (Lee et al., 2001) In particular, the fact that the distributed robust linear controller remarkably well suppressed near-wall turbulence in a turbulent flow opens another possibility of being able to be used in other various flows since it works even in the different basic plant rather than the plane Poiseuille flow, from which the controller is designed. This paper demonstrates that this can be successfully applied to control disturbance wall-shear stress in two-dimensional boundary layer flows.

In section 2, we derive the state-space equations from the linearized two-dimensional Navier-Stokes equations, reduce those order, and design a reduced-order two-dimensional linear controller by using linear-quadratic-Gaussian (LQG)/loop-transfer-recovery (LTR). In section 3, we present a numerical method. In section 4, we demonstrate how well the distributed linear robust controller can suppress disturbance wall-shear stress in linear and nonlinear boundary layer flows, followed by the conclusion.

In this paper, we use (u, v) to represent the velocity components in the streamwise (x) and wall-normal (y) directions, respectively, and (t) for the time.

2. Controller Design

In this section, we describe how the state-space equations are derived and the distributed linear controller is designed. To obtain the state-space equations as a basic model, we consider the two-dimensional linearized Navier-Stokes (N-S) equations in a plane Poiseuille flow, given in Fig. 1. The linearized N-S equations in terms of the disturbance streamfunction, $\psi(x, y, t)$, are written as

$$\left(\frac{\partial}{\partial t}+U\frac{\partial}{\partial x}\right)\Delta\psi-\frac{d^2U}{dy^2}\frac{\partial\psi}{\partial x}=\frac{1}{Re}\Delta\Delta\psi \qquad (1)$$

where Δ is the Laplacian operator. All the quantities are normalized by the channel half-height h and the centerline velocity U_c and U is an undisturbed velocity profile, $1-y^2$. Reynolds number Re is defined as $\frac{U_c h}{\nu}$ where ν is a kinematic viscosity. Considering blowing/suction only at the bottom wall as control input, the boundary conditions for ψ are

$$\frac{\partial\psi}{\partial x}(x, y=-1, t)=-v_w \qquad (2)$$

$$\frac{\partial\psi}{\partial x}(x, y=1, t)=\psi(x, y=\pm1, t)=0 \qquad (3)$$

The disturbance wall-shear stress as output measurement is expressed as

$$z(x, t)=\frac{\partial u}{\partial y}\bigg|_{y=-1}=\frac{\partial^2\psi}{\partial y^2}\bigg|_{y=-1}=0 \qquad (4)$$

An optimal performance index is essential in the LQG ($\mathbf{H}_2$) control design. We set a performance index such that both the near-wall disturbance and the controller cost are minimized. Knowing that the system can be operated away from the region, where a linear assumption holds, due to large control input, the controller cost is included in the performance index. Even though it is recommended to minimize the disturbance energy for the control of a system, it is very difficult to assess the energy that drives the system in many engineering problems. Because of the high correlation between the near-wall disturbance and the disturbance wall-shear stress, the disturbance wall-shear stress rather than the disturbance energy, instead, is included in defining the optimal performance index. The performance index is written as follows:

$$\Im=\lim_{t_f\to\infty}\int_t^{t_f}\int_0^{Lx}\left[\left(\frac{\partial u}{\partial y}\bigg|_w\right)^2+v_w^2\right]dxdt \qquad (5)$$

In order to obtain the state-space model from the partial differential equation with the boundary conditions and the output measurement, Eqs. (1-4), first, we decomposed all flow vari-

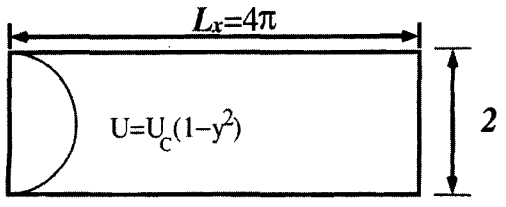

Fig. 1 Poiseuille channel flow configuration for the basis of controller design. U_c is the centerline velocity

ables spectrally by using periodic functions in the streamwise direction and Chebyshev polynomials in the wall-normal direction as

$$\psi(x, y, t)=\sum_{n=1}^{N}\sum_{m=1}^{M}[a_{nm}(t)\cos(\alpha_n x)+b_{nm}(t)\sin(\alpha_n x)]\Gamma_m(y) +\sum_{n=1}^{N}[p_n(t)\cos(\alpha_n x)+q_n(t)\sin(\alpha_n x)]f(y) \quad (6)$$

where $\alpha_n=2\pi n/L_x$. Functions Γ_m and f are the linear combinations of Chebyshev polynomials such that they satisfy the homogeneous boundary conditions and the given boundary conditions, Eqs. (2-3), respectively. The measurement equation, z, can be expanded as

$$z=\sum_{n=1}^{N}[c_n(t)\cos(\alpha_n x)+d_n(t)\sin(\alpha_n x)] \quad (7)$$

Second, we employed Galerkin projection and matrix transformation to reach the final form of the state-space variable (Lee et al., 2001 ; Lee, 1999):

$$\frac{d\mathbf{x}}{dt}=\mathbf{Ax}+\mathbf{Bu},\ \mathbf{z}=\mathbf{Cx}+\mathbf{Du} \quad (8)$$

where vectors **x**, **u**, and **z** represent the internal state, the control, and the measurement vectors, respectively. Note that matrices **A**, **B**, and **C** represent the dynamics of a plane Poiseuille flow, actuators, and sensors, respectively, while matrix **D** contains the direct coupling between sensors and actuators. The performance index, Eq. (5), can also be represented by

$$\Im=\lim_{t_f\to\infty}\int_t^{t_f}[\mathbf{z}^T\mathbf{z}+\mathbf{u}^T\mathbf{F}^T\mathbf{F}\mathbf{u}]dxdt \quad (9)$$

where the superscript T denotes a transposed quantity. The matrix **F** is obtained by spectrally decomposing the last term in the cost criterion, Eq. (5).

Since the linearized N-S equations are considered in this derivation, the system equation can be decomposed into N independent state-space subsystems (Cortelezzi and Speyer, 1998 ; Cortelezzi et al., 1998 ; Lee et al., 2001 ; Lee, 1999) Each individual state-space subsystem for a given wavenumber, α, is

$$\frac{d\mathbf{x}_\alpha}{dt}=\mathbf{A}_\alpha\mathbf{x}_\alpha+\mathbf{B}_\alpha\mathbf{u}_\alpha,\ \mathbf{z}_\alpha=\mathbf{C}_\alpha\mathbf{x}_\alpha+\mathbf{D}_\alpha\mathbf{u}_\alpha \quad (10)$$

with initial condition $\mathbf{x}_\alpha(0)=\mathbf{x}_{\alpha 0}$. Vectors $\mathbf{x}_\alpha$, $\mathbf{u}_\alpha$, and $\mathbf{z}_\alpha$ represent the internal, the control, and the output vectors for a given wavenumber α, respectively. Similarly, the characteristics of the linear system makes the cost functional, Eq. (9) which though contains quadratic terms, represented by a sum of N independent wavenumber cost functional, $\Im_\alpha$. The cost functional for a given wavenumber α is written as follows:

$$\Im_\alpha=\lim_{t_f\to\infty}\int_t^{t_f}[\mathbf{z}_\alpha{}^T\mathbf{z}_\alpha+\mathbf{u}_\alpha{}^T\mathbf{F}_\alpha{}^T\mathbf{F}_\alpha\mathbf{u}_\alpha]dxdt \quad (11)$$

Therefore, because of the independence of Eqs. (6-7) with respect to the wavenumber, the design of an optimal and robust controller for the system, Eq. (8), with Eq. (9) renders to the N independent robust single-wavenumber controller designs for the subsystem, Eq. (10), with its corresponding cost functional, Eq. (11).

Low-order controllers are usually preferred to high-order controllers since there are fewer things to have something wrong in hardware or bugs in software for the former than for the latter. Low-order controllers require lower cost of hardware construction as well as less computation time than high-order ones do. In order to construct the low-order controller, we first reduced the order of the system and designed a robust linear controller for the reduced-order model. For the reduced-order model, we transformed individual state-space subsystem, Eq. (10), into a Jordan Canonical form. From the transformed $\mathbf{B}_\alpha$ and $\mathbf{C}_\alpha$, the states that are equally well-controllable and-observable are chosen to constitute a reduced-order model, whose dynamics is represented by $\hat{\mathbf{A}}_\alpha$, $\hat{\mathbf{B}}_\alpha$, $\hat{\mathbf{C}}_\alpha$, and $\mathbf{D}_\alpha$. That is,

$$\frac{d\hat{\mathbf{x}}_\alpha}{dt}=\hat{\mathbf{A}}_\alpha\hat{\mathbf{x}}_\alpha,\ \hat{\mathbf{B}}_\alpha\mathbf{u}_\alpha,\ \hat{\mathbf{z}}_\alpha=\hat{\mathbf{C}}_\alpha\hat{\mathbf{x}}_\alpha+\mathbf{D}_\alpha\mathbf{u}_\alpha \quad (12)$$

where $\hat{\mathbf{x}}_\alpha$ is the reduced-order internal state vector and $\hat{\mathbf{z}}_\alpha$ is the measurement vector expressed in terms of $\hat{\mathbf{x}}_\alpha$. Similarly, we define a cost functional of the reduced-order model for a given wavenumber as follows:

$$\hat{\Im}_\alpha=\lim_{t_f\to\infty}\int_t^{t_f}[\hat{\mathbf{z}}_\alpha{}^T\hat{\mathbf{z}}_\alpha+\mathbf{u}_\alpha{}^T\mathbf{F}_\alpha{}^T\mathbf{F}_\alpha\mathbf{u}_\alpha]dxdt \quad (13)$$

For the design of rigorous controllers for N independent reduced-order models, we prefer **LQG** ($\mathbf{H}_2$) synthesis for this study eventhough a

rigorous mathematical framework for the design of disturbance attenuation ($\mathbf{H}_\infty$) linear controllers is available in the control synthesis theory. (Zhou et al., 1996) A brief review on **LQG** ($\mathbf{H}_2$) synthesis of a particular wavenumber will be given in a self-contained manner.

The LQG problem as a stochastic optimal control problem is formulated by

$$\dot{\hat{\mathbf{x}}}_\alpha=\hat{\mathbf{A}}_\alpha\hat{\mathbf{x}}_\alpha+\hat{\mathbf{B}}_\alpha\mathbf{u}_\alpha+\boldsymbol{\Gamma}_\alpha\mathbf{w}_\alpha \tag{14}$$

$$\hat{\mathbf{z}}_\alpha=\hat{\mathbf{C}}_\alpha\hat{\mathbf{x}}_\alpha+\mathbf{D}_\alpha\mathbf{u}_\alpha+\mathbf{v}_\alpha \tag{15}$$

where $\boldsymbol{\Gamma}_\alpha$ is an input matrix, $\mathbf{w}_\alpha$ and $\mathbf{v}_\alpha$ are both white Gaussian noise processes with zero means and auto-correlation functions

$$\begin{aligned}E[\mathbf{w}_\alpha(t)\mathbf{w}_\alpha^T(\tau)]&=\mathbf{W}_\alpha\delta(t-\tau)\\ E[\mathbf{v}_\alpha(t)\mathbf{v}_\alpha^T(\tau)]&=\mathbf{V}_\alpha\delta(t-\tau)\end{aligned} \tag{16}$$

where $E[\cdot]$ is the expectation operator averaging over all underlying random variables and $\delta(t-\tau)$ is the delta function. Note that $\mathbf{W}_\alpha$ and $\mathbf{V}_\alpha$, the power spectral densities, will be chosen here as design parameters to enhance system performance. Additional comments on the controller design process will be given at the end of this section.

The LQG controller is determined by finding the control action $\mathbf{u}_\alpha(Z_t)$, where $Z_t=\{z(\tau)\ ;\ 0\le\tau\le t\}$ is the measurement history, which minimizes the cost criterion

$$J_\alpha=\lim_{t_f\to\infty}\frac{1}{t_f-t}E\left[\int_t^{t_f}(\hat{\mathbf{x}}_\alpha^T\mathbf{Q}_\alpha\hat{\mathbf{x}}_\alpha+2\hat{\mathbf{x}}_\alpha^T\mathbf{N}_\alpha\hat{\mathbf{u}}_\alpha+\hat{\mathbf{u}}_\alpha^T\mathbf{R}_\alpha\hat{\mathbf{u}}_\alpha)\,d\tau\right] \tag{17}$$

subject to the stochastic dynamic system model Eqs. (15-16). Note that, from Eqs. (12-13), $\mathbf{Q}_\alpha=\hat{\mathbf{C}}_\alpha^T\hat{\mathbf{C}}_\alpha$, $\mathbf{N}_\alpha=\hat{\mathbf{C}}_\alpha^T\mathbf{D}_\alpha$, and $\mathbf{R}_\alpha=\mathbf{D}_\alpha^T\mathbf{D}_\alpha+\mathbf{F}_\alpha^T\mathbf{F}_\alpha$. The division by (t_f-t) ensures that the cost criterion remains finite in the presence of uncertainties in the infinite-time problem ($t_f\to\infty$). Note that Eq. (17) can include Eq. (13) where

$$J_\alpha=\lim_{t_f\to\infty}\frac{1}{t_f-t}E[\mathfrak{I}_\alpha] \tag{18}$$

and the limit in Eq. (13) is explicitly denoted in Eq. (18). Note that even though the time interval is infinite, time response is still measured by the eigenvalues of the closed-loop system. We consider the infinite-time problem with a time-invariant dynamics because the controller gains become constants.

By nesting the conditional expectation with respect to Z_t within the unconditional expectation of Eq. (18), i.e., $E[\mathfrak{I}_\alpha]=E[E[\mathfrak{I}_\alpha/Z_t]]$ where $E[\cdot/Z_t]$ denotes the expectation of $(\cdot)$ conditioned on Z_t, the cost criterion can be written as

$$\begin{aligned}J_\alpha=\lim_{t_f\to\infty}\frac{1}{t_f-t}E\Big[\int_t^{t_f}[&(\tilde{\mathbf{x}}_\alpha^T\mathbf{Q}_\alpha\tilde{\mathbf{x}}_\alpha\\ &+2\hat{\mathbf{x}}_\alpha^T\mathbf{N}_\alpha\mathbf{u}_\alpha+\mathbf{u}_\alpha^T\mathbf{R}_\alpha\mathbf{u}_\alpha+tr(\mathbf{P}_\alpha)]\,d\tau\Big]\end{aligned} \tag{19}$$

where $\tilde{\mathbf{x}}_\alpha=E[\hat{\mathbf{x}}_\alpha/Z_t]$ is the conditional mean estimate of the state $\hat{\mathbf{x}}_\alpha$ and $\mathbf{P}_\alpha$ is the conditional error covariance matrix with to $\tilde{\mathbf{x}}_\alpha$. This cost criterion is now minimized subject to the estimation equations discussed below. Note that $\mathbf{P}_\alpha$ does not depend on the control (see Eq. (23) below) and therefore, does not enter into the optimization process.

The solution to the regulator problem (Kwakernaak and Silvan, 1969) is a compensator composed of a state reconstruction process, known here as a filter (in the no-noise case it is known as an observer) in cascade with a controller (see Fig. 2 where E_i is the estimator and C_i is the

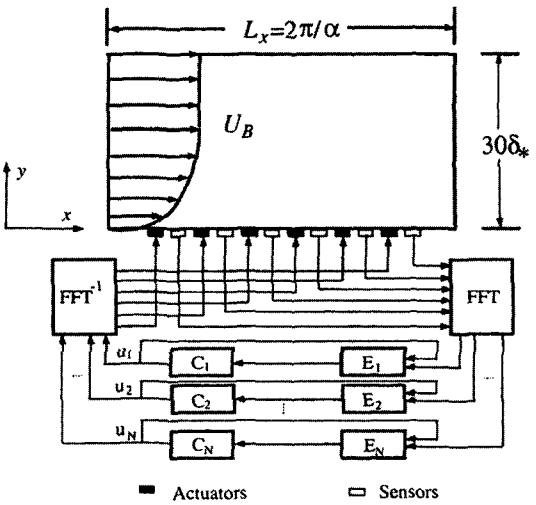

Fig. 2 Boundary layer flow equipped with distributed sensors and controllers. C_i and E_i represent the controller and the estimator, respectively. U_B, α, and δ_* stand for the Blasius boundary layer velocity profile, the wavenumber, and the displacement thickness, respectively

controller). The state estimate (conditional mean) $\tilde{\mathbf{x}}_\alpha$ is governed by the so-called Kalman filter as

$$\begin{aligned}\dot{\tilde{\mathbf{x}}}_\alpha &= \hat{\mathbf{A}}_\alpha\tilde{\mathbf{x}}_\alpha+\hat{\mathbf{B}}_\alpha\mathbf{u}_\alpha+\hat{\mathbf{L}}_\alpha\nu_\alpha,\\ \nu_\alpha &= \hat{\mathbf{z}}_\alpha-\tilde{\mathbf{z}}_\alpha=\hat{\mathbf{C}}_\alpha(\hat{\mathbf{x}}_\alpha-\tilde{\mathbf{x}}_\alpha)+\mathbf{v}_\alpha\end{aligned} \tag{20}$$

If the reduced-order system were the actual system, then ν_α in Eq. (20) is correct. When the actual system is considered and the filter is implemented based on the reduced-state-space, $\mathbf{z}$ rather than $\hat{\mathbf{z}}$ is the measurement and the filter residual becomes

$$\nu_\alpha=\mathbf{z}_\alpha-\hat{\mathbf{C}}_\alpha\tilde{\mathbf{x}}_\alpha-\mathbf{D}_\alpha\mathbf{u}_\alpha \tag{21}$$

The Kalman gain matrix $\hat{\mathbf{L}}_\alpha$, constructed to trade the accuracy of the new measurements against the accuracy of the state propagated from the system dynamics, is given by

$$\hat{\mathbf{L}}_\alpha=\mathbf{P}_\alpha\hat{\mathbf{C}}_\alpha^T\mathbf{V}_\alpha^{-1} \tag{22}$$

where $\mathbf{P}_\alpha$ is the error covariance matrix in the statistical problem.

In the infinite-time stationary formulation, the $\mathbf{P}_\alpha$ is the solution to the algebraic Riccati equation (ARE),

$$\hat{\mathbf{A}}_\alpha^T\mathbf{P}_\alpha+\mathbf{P}_\alpha\hat{\mathbf{A}}_\alpha+\boldsymbol{\Gamma}_\alpha\mathbf{W}_\alpha\boldsymbol{\Gamma}_\alpha^T-\mathbf{P}_\alpha\hat{\mathbf{C}}_\alpha^T\mathbf{V}_\alpha^{-1}\hat{\mathbf{C}}_\alpha\mathbf{P}_\alpha=0 \tag{23}$$

If the system is $(\hat{\mathbf{A}}_\alpha, \hat{\mathbf{C}}_\alpha)$ observable and $(\hat{\mathbf{A}}_\alpha, \hat{\mathbf{B}}_\alpha)$ controllable, then $\mathbf{P}_\alpha$ is positive definite. Under these assumptions, it can be shown that the difference between the internal state $\hat{\mathbf{x}}_\alpha$ and the estimate state $\tilde{\mathbf{x}}_\alpha$, i.e., the error

$$\mathbf{e}_\alpha=\hat{\mathbf{x}}_\alpha-\tilde{\mathbf{x}}_\alpha \tag{24}$$

goes to zero as time goes to infinity. In other words, the evolution equation

$$\dot{\mathbf{e}}_\alpha=\mathbf{A}_f\mathbf{e}_\alpha+\hat{\mathbf{L}}_\alpha\nu_\alpha+\hat{\boldsymbol{\Gamma}}_\alpha\mathbf{w}_\alpha \tag{25}$$

is stable, i.e., all the eigenvalues of the matrix

$$\mathbf{A}_f=\hat{\mathbf{A}}_\alpha-\hat{\mathbf{L}}_\alpha\hat{\mathbf{C}}_\alpha \tag{26}$$

have negative real parts.

Minimizing the infinite-time cost function J, Eq. (19) subject to Eq. (20) yields the following control law,

$$\mathbf{u}_\alpha=-\hat{\mathbf{K}}_\alpha\tilde{\mathbf{x}}_\alpha \tag{27}$$

where

$$\hat{\mathbf{K}}_\alpha=\mathbf{R}_\alpha^{-1}(\hat{\mathbf{B}}_\alpha^T\mathbf{S}_\alpha+\mathbf{N}_\alpha) \tag{28}$$

and $\mathbf{S}_\alpha$ is the solution of the algebraic Riccati equation (ARE)

$$\hat{\mathbf{A}}_\alpha^T\mathbf{S}_\alpha+\mathbf{S}_\alpha\hat{\mathbf{A}}_\alpha+\mathbf{Q}_\alpha-(\mathbf{S}_\alpha\hat{\mathbf{B}}_\alpha+\mathbf{N}_\alpha)\mathbf{R}_\alpha^{-1}(\hat{\mathbf{B}}_\alpha^T\mathbf{S}_\alpha+\mathbf{N}_\alpha^T)=0 \tag{29}$$

It should be remarked that the control gain matrix $\hat{\mathbf{K}}_\alpha$ is determined from functions only of the known dynamics coefficients $(\hat{\mathbf{A}}_\alpha, \hat{\mathbf{B}}_\alpha)$ and the weighting in the cost criterion $(\mathbf{Q}_\alpha, \mathbf{R}_\alpha)$, and not the statistics of the input $(\mathbf{V}_\alpha, \mathbf{W}_\alpha)$. Consequently, $\hat{\mathbf{K}}_\alpha$ is determined from a performance index as Eq. (17), independent of the stochastic inputs. If $(\hat{\mathbf{A}}_\alpha, \hat{\mathbf{B}}_\alpha)$ is controllable and $(\hat{\mathbf{A}}_\alpha, \mathbf{Q}_\alpha^{1/2})$ observable, then the loop coefficient matrix

$$\mathbf{A}_c=\hat{\mathbf{A}}_\alpha-\hat{\mathbf{K}}_\alpha\hat{\mathbf{B}}_\alpha \tag{30}$$

is stable and $\mathbf{S}_\alpha$ is positive definite. The controllable and observable conditions can be weakened to be stabilizable and detectable (Kwakernaak and Silvan, 1969).

When we combine the estimator and the regulator together, the dynamic system composed of the controlled process and filter becomes

$$\begin{pmatrix}\mathbf{e}_\alpha\\ \dot{\tilde{\mathbf{x}}}_\alpha\end{pmatrix}=\begin{bmatrix}\mathbf{A}_f & 0\\ \hat{\mathbf{L}}_\alpha\hat{\mathbf{C}}_\alpha & \mathbf{A}_c\end{bmatrix}\begin{pmatrix}\mathbf{e}_\alpha\\ \tilde{\mathbf{x}}_\alpha\end{pmatrix}+\begin{pmatrix}\hat{\mathbf{L}}_\alpha\mathbf{v}_\alpha+\boldsymbol{\Gamma}_\alpha\mathbf{w}_\alpha\\ \hat{\mathbf{L}}_\alpha\mathbf{v}_\alpha\end{pmatrix} \tag{31}$$

Note that any choice of two between $\mathbf{e}$, $\hat{\mathbf{x}}_\alpha$, and, $\tilde{\mathbf{x}}_\alpha$ produces the same dynamics because they are algebraically related by Eq. (24). Under the above controllability and observability assumptions, $\mathbf{A}_f$ and $\mathbf{A}_c$ have only stable eigenvalues if optimal gains $\hat{\mathbf{L}}_\alpha$ and $\hat{\mathbf{K}}_\alpha$ of Eqs. (22) and (28) are used. If the actual linear system is used, then $\mathbf{x}_\alpha$ and the reduced-order state estimate $\tilde{\mathbf{x}}_\alpha$ are used to form the closed-loop dynamic system rather than that given in Eq. (31). The eigenvalues of the dynamical matrix now dictate the system stability and will differ from the ideal case of Eq. (31).

The parameters used in our LQG design are now addressed. Since the power spectral density is not known, for simplicity of the design we consider $\mathbf{V}_\alpha$ and $\mathbf{W}_\alpha$ to be of the form $\mathbf{V}_\alpha=\beta\mathbf{I}$ and $\mathbf{W}_\alpha=\rho\mathbf{I}$ where β and ρ are scalars and $\mathbf{I}$ is an identity matrix. Only the ratio of β and ρ is important. Furthermore, by choosing $\boldsymbol{\Gamma}_\alpha=\hat{\mathbf{B}}_\alpha$, loop-transfer-recovery (LTR) of the LQG controller to full-state feedback (Zhou et al., 1996) guarantees that robust performance occurs when the process noise power spectral density goes to infinity, i.e., $\rho\rightarrow\infty$, provided there exists no

nonminimal-phase zero in the plant. In our case, there are no nonminimal-phase zeros. Robust performance means 60° of phase margin and at least 6 db of gain margin. Note that the choice of $\boldsymbol{\Gamma}_a=\hat{\mathbf{B}}_a$ implies that the noise is generated along the wall as is the control and could be interpreted as due to wall roughness. Furthermore, the values of ρ and $\mathbf{W}_a$ were determined by tuning the controller in the presence of nonlinear flow. The degree of loop transfer recovery varied from controller to controller.

As described above using LQG/LTR assumes that the uncertainty is at the wall and affects the dynamics in the same way as the control. This is more physically motivated than the uncertainty structure assumed by Bewley and Liu (1998) where uncertainty is assumed uniformly throughout the channel. Furthermore, robustness in terms of traditional measures of gain and phase margins in control engineering are also obtained by using LQG/LTR. For these reasons, the LQG/LTR is preferred over the unstructured uncertainty $\boldsymbol{H}_\infty$ controllers.

Figure 2 represents the boundary layer flow installed with distributed sensors and controllers by summarizing in a block diagram the control strategy described above. The computer program of two-dimensional distributed controller/sensor whose input is the matrix containing the gradients of the streamwise velocity component and whose output is the matrix containing the blowing and suction at the wall is embedded in our simulation program. The measured streamwise disturbance gradient is transformed to $\mathbf{z}_a$'s by fast Fourier transform (FFT). Each single wavenumber controller is integrated in time by a third-order low-storage Runge-Kutta scheme to generate the input $\mathbf{u}_a$'s. An inverse FFT converts $\mathbf{u}_a$'s into real blowing/suction according to the last summation term of Eq. (6).

This real blowing/suction is distributed along the streamwise wall.

3. Numerical Method

A two-dimensional parallel periodic boundary layer flow with a Blasius mean velocity profile (U_B), given in Fig. 2, is taken as the model flow for our control study of transition. All variables are nondimensionalized with free stream velocity, U_∞, and the displacement thickness, $\delta_*=\int_0^\infty\left(1-\frac{U}{U_\infty}\right)dy$. Also, the Reynolds number is defined as $Re_{\delta_*}=\frac{U_\infty\delta_*}{\nu}$. In our numerical simulation, δ_* and Re_{δ_*} are kept constant, assuming the boundary layer thickness does not vary in the streamwise direction. The time-dependent incompressible N-S equations in a two-dimensional boundary layer flow are

$$\frac{\partial u_i}{\partial t}+u_j\frac{\partial u_i}{\partial x_j}=-\frac{\partial p}{\partial x}+\frac{1}{Re_{\delta_*}}\frac{\partial^2 u_i}{\partial x_j\partial x_j}+g\delta_{i,1},\quad i,j=1,2 \tag{32}$$

where u_1 and u_2 represent the streamwise and wall-normal velocities, respectively, and $\delta_{i,1}$ is the Kroneker delta function.

The forcing term, g, given by $\frac{1}{Re_{\delta_*}}\frac{d^2U}{dy^2}$, is introduced so that the initial Blasius profile $U_B(y)$ is preserved in the simulation (Zang and Hussaini, 1985; Laurien and Kleiser, 1986).

For the present study, uniform grid spacing is used in the streamwise direction, while nonuniform grid spacing is adopted in the wall-normal direction. In order to generate the nonuniform grid spacing in the wall-normal direction, we use a transformation function defined by

$$y(\eta)=\frac{y_{\max}\sigma\eta}{\eta_{\max}\sigma+y_{\max}(\eta_{\max}-\eta)} \tag{33}$$

where $y_{\max}$ is the height of physical domain, $\eta_{\max}$ is the height of computational domain, and σ is a constant that determines the concentration of grid-points near the wall. σ is chosen such that the numerical solution for small disturbance is matched with Linear Stability Theory (LST). For the spatial discretization of Eq. (32), the fourth-order compact finite difference scheme (Lele, 1992) is used on the staggered grid.

For time advancement, we use a fractional step method suggested by Le and Moin(1991). The time integration is carried out with the 3rd order Runge-Kutta (RK) scheme for the nonlinear term and 2nd order Crank-Nicolson one for the

viscous term. The velocity field is time-advanced through each RK substep without satisfying continuity. The velocities are projected onto the divergence-free field only at the last RK substep. In this paper, we use a modification of Le and Moin' s method, described by

$$\frac{\tilde{u}_i^{(l)}-\tilde{u}_i^{(l-1)}}{\Delta t}=(\alpha_l+\beta_l)L(\tilde{u}_i^{(l-1)})-\frac{\alpha_l}{Re_\delta}\frac{\partial}{\partial x_i}\left(\frac{\partial \tilde{u}_k^{(l-1)}}{\partial x_k}\right)$$
$$+\beta_l L(\tilde{u}_i^{(l)}-\tilde{u}_i^{(l-1)})-\gamma_l N(u_i^{*(l-1)}) \quad (34)$$
$$-\varsigma_l N(u_i^{*(l-2)})-(\alpha_l+\beta_l)\frac{\partial P^n}{\partial x_i},\ i=1,2$$

where $\tilde{u}_i^{(l)}$ denotes the intermediate velocity components (not satisfying the continuity equation) of each RK substep; $\tilde{u}_i^{*(l)}$ is the modified velocity in the convective terms to maintain the order of accuracy of the scheme; the superscript $l(=1, 2, 3)$ indicates the RK substep; n represents the previous time; $L(u_i)$ and $N(u_i)$ represent the 4th-order compact finite difference operators to approximate the viscous and convective terms, respectively. Note that the coefficients α_l, β_l, γ_l, and ς_l are constants such that the total time advancement between t^n and t^{n+1} is third-order accurate for the convective terms and second-order accurate for the viscous terms. The boundary condition of the intermediate velocity, $\tilde{u}_i^{(l)}$, can be approximated by

$$\tilde{u}_i^{(l)}=u_i^{n+1}+\vartheta(\Delta t^2),\ l=1, 2, 3 \quad (35)$$

At the last RK substep ($l=3$), Poisson equation is obtained by enforcing the divergence-free constraint below:

$$\frac{\partial^2\phi}{\partial x_k\partial x_k}=\frac{1}{\Delta t}\frac{\partial \tilde{u}_k^{(3)}}{\partial x_k} \quad (36)$$

Once ϕ is obtained, the divergence-free velocity components at time step $n+1$ can be obtained from the relationship:

$$u_i^{n+1}=\tilde{u}_i^{(3)}-\Delta t\frac{\partial\phi}{\partial x_i} \quad (37)$$

Poisson equation, Eq. (36), approximated with the 2nd-order central difference method, is solved by a direct Poisson solver (Door, 1970; 1973; Kim and Moin, 1985; Schumann and Sweet, 1988). In this paper, we use the Kim and Moin's algorithm (1985) incorporated with FFT.

4. Results

Prior to a direct application of our controller to the boundary layer flow we consider as a plant, we have checked the validity of our order reduction method. In this process, we performed the linear stability in the channel flow with Re=1500 and $\alpha=1.0$ and verified our order reduction method through the outputs in the full system (Eq. (10):122 states) and the reduced-order system (Eq. (12):12 states). Figure 3 shows that the both outputs are in excellent agreement. This backs it up that our order reduction is well carried out.

We have designed a reduced-order controller for two-dimensional Poiseuille flow in a channel of $L_x=4\pi$ at Re=1500 with the grid resolution of $N=32$ and $M=60$. We reduced the order of the controller by 90% from 122 states of the full-order system, Eq. (10), to 12 states of the reduced-order system, Eq. (12), for each wavenumber. For a numerical simulation, a finite difference direct numerical simulation has been carried out. Two different instability cases have been selected for the study: linear Tollmien-Schlichting instability and nonlinear disturbances in

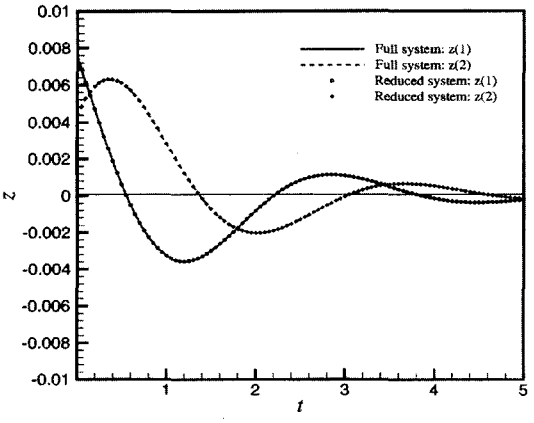

Fig. 3 Comparison of outputs between the full and reduced systems. Linear stability outputs in the channel flow at $Re=1500$ and $\alpha=1.0$. Symbols and lines represent the output behaviors of the reduced-order and full-order systems, respectively

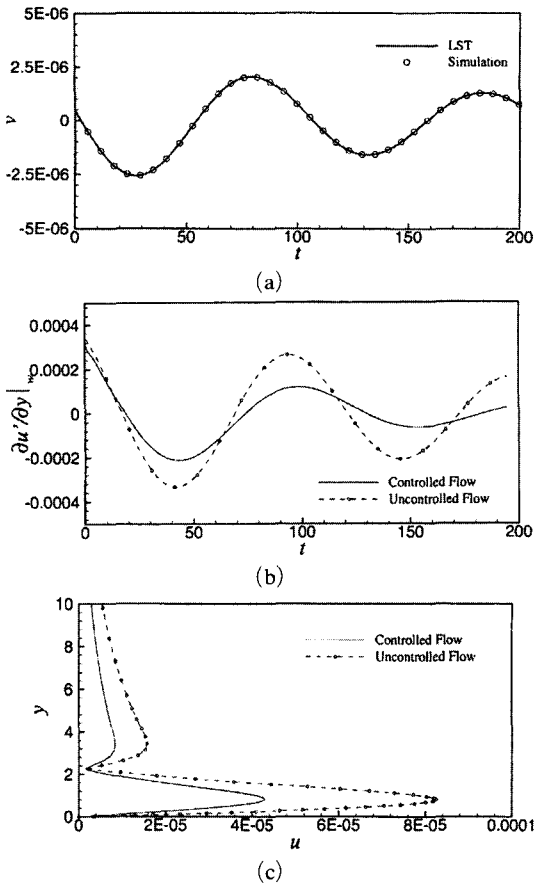

Fig. 4 Control of linear stability flow at $Re_{\delta*}=516$ and $\alpha=0.172$: (a) The wall-normal velocity compared with linear stability theory; (b) The comparison of disturbance wall-shear stresses at particular location between controlled and uncontrolled flows; (c) Comparison of the streamwise eigenfunctions at $t=120$ between controlled and uncontrolled flows

the boundary layer flows. These selective tests will be served to give extensive robustness, in the sense of control performance, of the controller in the Blasius boundary layer flows.

4.1 Control of two-dimensional tollmien-schlichting wave

For this case, we assumed the initial velocity field in the form of

$$\mathbf{u}(x, y, t=0)=U_B(y)+A_m\mathrm{Re}(\hat{\mathbf{u}}(y)\,e^{i\alpha x}) \quad (38)$$

where $\hat{\mathbf{u}}(y)$ is the least stable or unstable eigenfunction of Orr-Sommerfeld (O-S) solution for a given $Re_{\delta*}$ and wavenumber α, i is $\sqrt{-1}$, and A_m is an amplitude of linear disturbance. Note that $\hat{\mathbf{u}}(y)$ is normalized such that the maximum value of the streamwise eigenfunction becomes unity.

We choose the simulation parameters $Re_{\delta*}=516$ (which is equivalent to $Re=1500$ used in the controller design) and $\alpha=0.172$. From the linear stability theory, the least stable eigenvalue for the Blasius boundary layer flow is $\omega=0.604-0.0045i$. The initial disturbance amplitude is $A_m=0.0001$. Although this disturbance will decay very slowly with the amplification rate of -0.0045, we can test the capability of the controller to suppress the wall-shear stress in the other basic plant than a Poiseuille channel flow from which the controller is designed. The computational domain is given by $\frac{2\pi}{\alpha}$ and $30\delta_*$ in the streamwise and wall-normal directions, respectively.

To demonstrate the accuracy of our numerical method, we compared the results with linear stability theory in Fig. 4(a). The wall-normal velocity at a particular point in the uncontrolled flow is in excellent agreement with LST. Figure 4(b) shows a comparison of the disturbance wall-shear stresses in the controlled and uncontrolled flows. The disturbance wall-shear stress in the controlled flow decays even faster than in the uncontrolled flow due to the controller, accompanying the short transient response as soon as the controller is on. It indicates that the closed-loop flow system equipped with our reduced-order controller has shifted the system pole of the uncontrolled flow system farther to the left hand side of complex plane like Joshi et al. (1997) showed. Figure 4(c) presents the comparison of the streamwise eigenfunctions in the controlled and uncontrolled flows at $t=120$, indicating that the whole flow field is affected uniformly due to the blowing/suction at the wall.

We applied our distributed reduced-order controller to another linear instability flow with $Re_{\delta*}=900$ and $\alpha=0.25$, which gives an unstable disturbance with the amplification rate of 0.0026

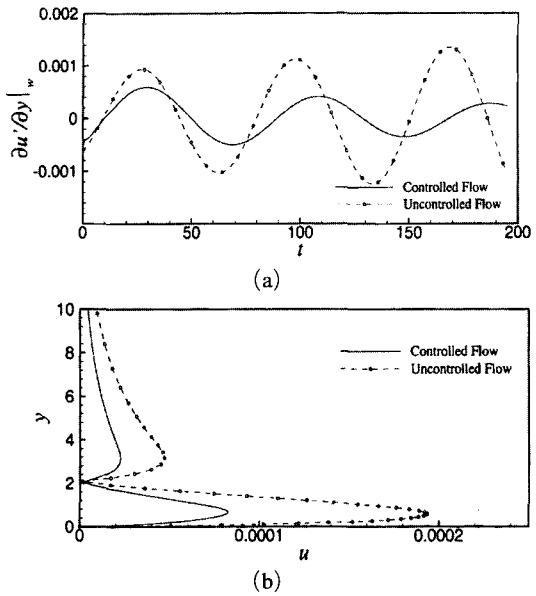

Fig. 5 Control of linear stability flow at $Re_{\delta*}=900$ and $\alpha=0.25$: (a) The comparison of disturbance wall-shear stresses at particular location between controlled and uncontrolled flows; (b) Comparison of the streamwise eigenfunctions at $t=120$ between controlled and uncontrolled flows

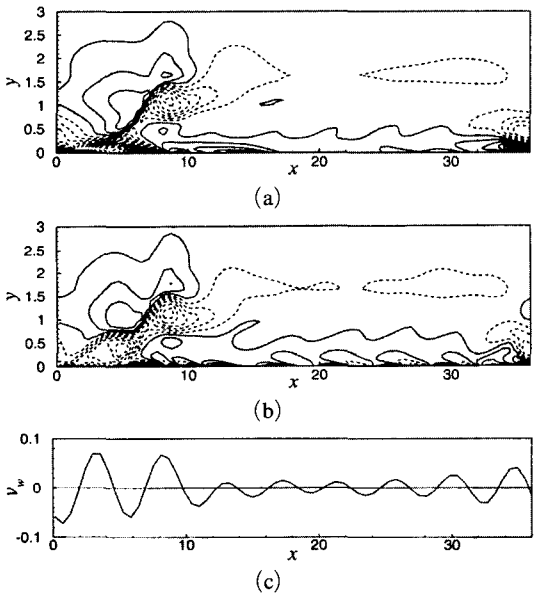

Fig. 6 Contours of the disturbance spanwise vorticity at $t=10$: (a) Uncontrolled flow; (b) Controlled flow; (c) v_{wall} along the wall. Negative contours are dotted

($\omega=0.089+0.0026$). Figure 5(a) shows a comparison of the disturbance wall-shear stresses in the controlled and uncontrolled flows. For the uncontrolled flow, the disturbance wall-shear stress is amplified with the theoretical amplification rate. In the controlled flow, however, the disturbance wall-shear stress decays in time, with accompanying the short transient response in the very early stage of control. Figure 5(b) also shows the effect of the controller on the streamwise eigenfunction at $t=120$, which shows that the flow field is uniformly affected. It can be said that, for linear disturbances, our two-dimensional linear controller designed from a plane Poiseuille channel flow works robustly against the Blasius boundary layer flows with various Reynolds numbers.

4.2 Control of nonlinear disturbance

We tested our controller in a two-dimensional nonlinear Blasius boundary layer flow at $\mathrm{Re}_{\delta*}=516$. For an initial nonlinear velocity field, we superpose the least stable eigenfunctions of O-S solution ranging from $\alpha_1=0.172$ to $\alpha_8=1.376$. That is, it is given by

$$\mathbf{u}(x, y, t=0)=U_B(y)+\mathrm{Re}\left(\sum_{n=1}^{n=8} A_n\hat{\mathbf{u}}_n(y)\,e^{i\alpha_n x}\right) \quad (39)$$

where disturbance amplitude A_n corresponding to wavenumber α_n, which has a decreasing spectrum in n, is chosen such that the initial disturbance velocity field has a maximum root-mean-square (rms) of $u'_{\mathrm{rms}}=0.1$, i.e., 10% of the free stream velocity. It will be shown later that its initial condition is enough to represent the nonlinear behavior of the flow. Note that the nonlinear effect of the initial velocity field is not at all taken to consideration in designing the distributed reduced-order linear controller, so that it can not be directly controlled.

Figures 6 and 7 show contours of the disturbance spanwise vorticity in the controlled and uncontrolled flows as well as blowing/suction applied at the wall at $t=10$ and 20. In the uncontrolled flow at $t=10$, the vortical structure outside the displacement thickness starts to take apart from one inside the displacement thickness.

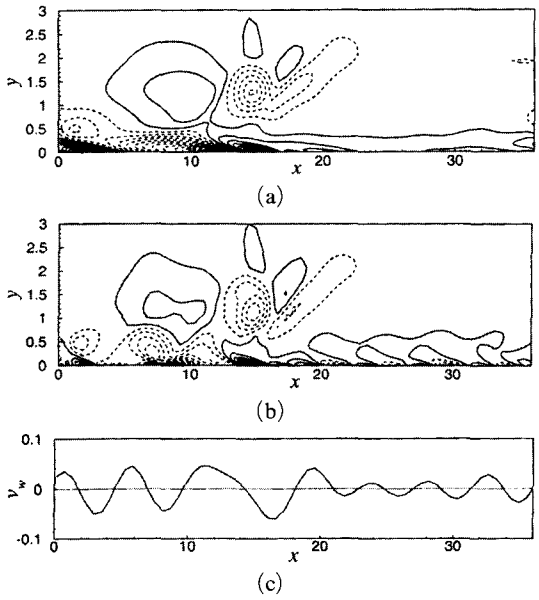

Fig. 7 Contours of the disturbance spanwise vorticity at $t=20$: (a) Uncontrolled flow; (b) Controlled flow; (c) v_{wall} along the wall. Negative contours are dotted

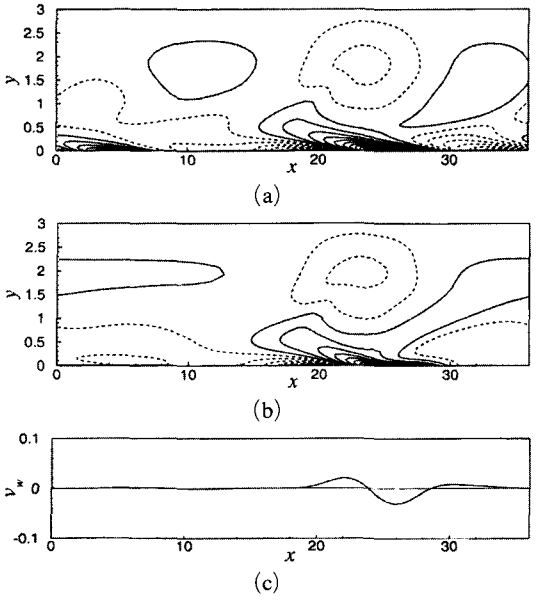

Fig. 8 Contours of the disturbance spanwise vorticity at $t=200$: (a) Uncontrolled flow; (b) Controlled flow; (c) v_{wall} along the wall. Negative contours are dotted

Strong negative and positive vorticity Field inside the displacement thickness alternates far upstream and far downstream, respectively. At $t=20$, the vortical structure outside the displacement thickness is getting isolated from one inside the displacement thickness. The strong positive and negative vortical structures are observed inside the half-displacement thickness.

For the controlled flow at $t=10$, the effect of the controller on the flow field is limited inside the displacement thickness. While the vortical structure outside the displacement thickness is changed little compared with the uncontrolled flow, the strength of the spanwise vorticity inside the displacement thickness is weaken. Due to the nonlinear interaction with the blowing/suction, moreover, small-valued-positive and-negative vortices near the wall alternate downstream. Figure 6(c) shows that the controller produces strong blowing/suction upstream and weak one downstream, depending on the disturbance wall-shear measurement. At $t=20$, the effect of the controller has penetrated into higher location than at $t=10$. The vortical structure outside the displacement thickness is lifted to form an isolated structure from one inside the displacement thickness. The spanwise vorticity near the wall is getting a bit larger than that at $t=10$. Also, the controller produces strong v_{wall} over the wider upstream than at $t=10$.

Figure 8 presents contours of the spanwise vorticity in the controlled and uncontrolled flows at $t=200$. It shows the blowing/suction applied at the wall as well. In the uncontrolled flow, the vortical structure outside the displacement thickness is separated from one inside the displacement thickness. The vortical structure inside the displacement thickness is distributed more regularly. In the controlled flow, the flow field is much affected by the controller. In particular, the spanwise vorticity inside the displacement thickness is greatly reduced compared with that of the uncontrolled flow. While the controller produces blowing velocity where the negative wall vorticity is detected, it generates suction velocity where the positive vorticity is observed.

Figures 9 and 10 show not only the spanwise vorticity contours in the controlled and uncon-

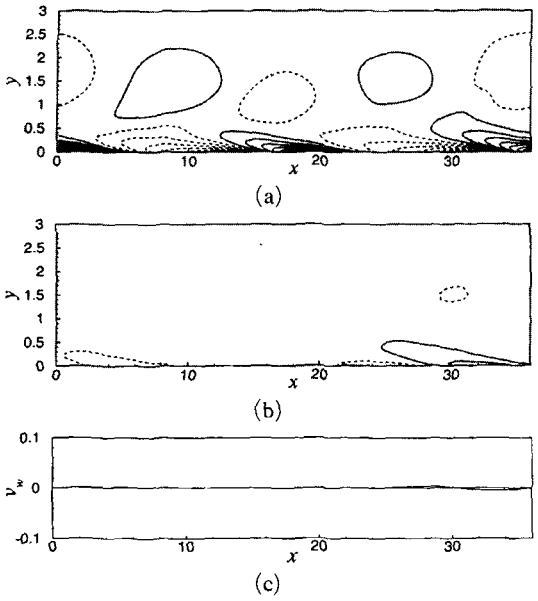

Fig. 9 Contours of the disturbance spanwise vorticity at $t=400$: (a) Uncontrolled flow; (b) Controlled flow; (c) v_{wall} along the wall. Negative contours are dotted

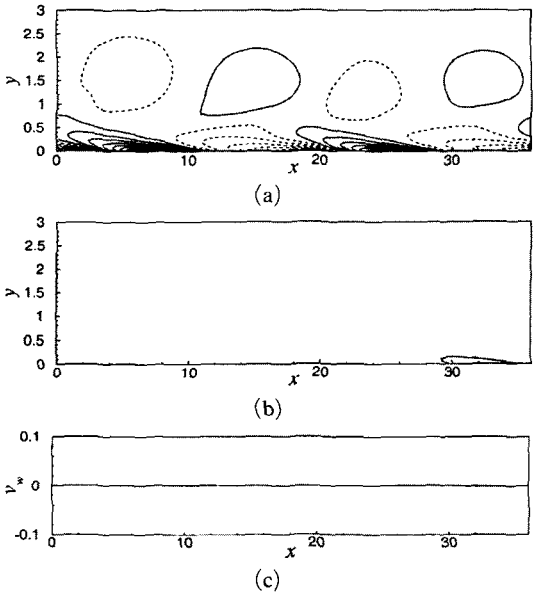

Fig. 10 Contours of the disturbance spanwise vorticity at $t=500$: (a) Uncontrolled flow; (b) Controlled flow; (c) v_{wall} along the wall. *Negative contours are dotted*

trolled flows, but also the blowing/suction applied at the wall, respectively, at $t=400$ and 500.

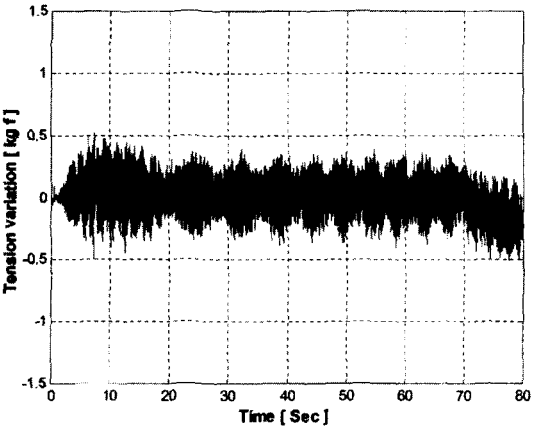

Fig. 11 Time evolution of disturbance wall-shear stresses at a given point in the controlled and uncontrolled flows: ———, uncontrolled flow; --○--, *controlled flow*

In the uncontrolled flow, the positive and negative vortical structures alternate regularly along the downstream and those strength increases slightly because of a nonlinear effect as time goes on, indicating that the resulting flow becomes unstable. Note that the eigenfunctions, $\hat{\mathbf{u}}_n(y)$ in Eq. (37), are stable for the linear disturbance with a given subcritical Reynolds number. In the controlled flow, most remaining vortical structures die out due to the controller as time goes on. The effect of the controller penetrates into the flow field far away from the boundary layer. The controller, correspondingly, produces almost zero blowing/suction velocity at the wall.

The time history of the disturbance wall-shear stresses in the controlled and uncontrolled flows is presented in Fig. 11. The disturbance wall-shear stress is measured at a given point. After a certain transient period, the reduced-order linear controller suppresses remarkably the wall-shear stress even in the nonlinear flow. It is interesting to note that the steady-state response of the wall-shear stress in the uncontrolled flow is amplified slowly. The observation is very consistent with Figs. 6-10.

For identification of the effect of each single-wavenumber controller on the wall-shear stress, the time history of the magnitude of Fourier coefficients of the wall-shear stresses in the con-

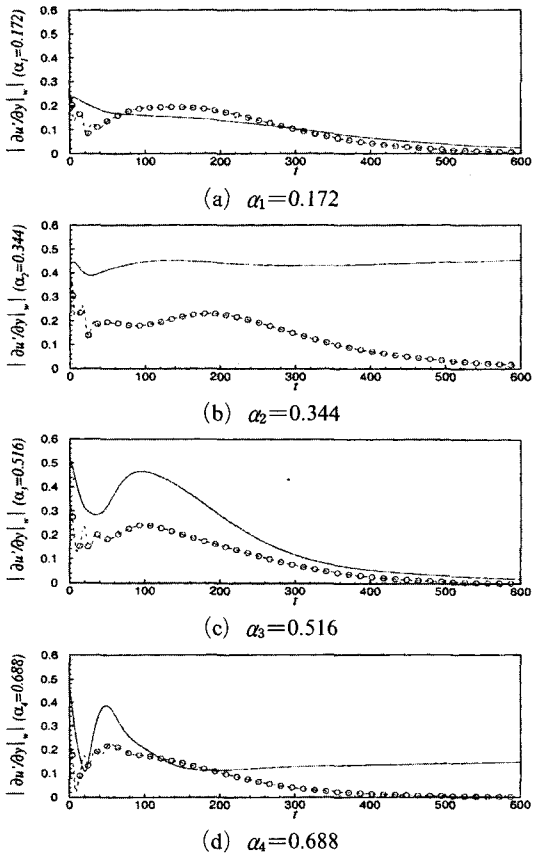

Fig. 12 Time evolution of the magnitude of Fourier coefficient of wall-shear stresses in the uncontrolled and controlled flows: ———, uncontrolled flow; --o--, controlled flow

trolled and uncontrolled flows is plotted in Fig. 12. The magnitude of Fourier coefficients of the wall-shear stress, corresponding to α_n=0.172, 0.516, ..., 1.204, decreases with time, irrespective of the controlled or uncontrolled flows. The magnitude in the controlled flow is though, in general, decayed more rapidly compared with that in the uncontrolled flow. For the components corresponding to α_n=0.344, 0.688, ..., 1.376 in the uncontrolled flow, the magnitudes increase slowly with time later than t=150, leading to a flow instability. It demonstrates that the initial condition is really nonlinear since all these components should die out at this subcritical Reynolds number if it is linear. These corresponding components in the controlled flow are, however, highly reduced in time to decay out. It is demonstrated that the linear reduced-order controller is working robustly against the finite amplitude disturbances in a different basic plant other than a plane Poiseuille channel flow.

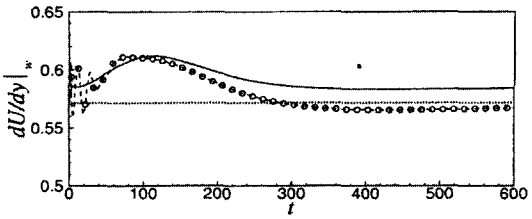

Fig. 13 Comparison of the viscous drag measured at the wall: ·····, laminar Blasius boundary layer flow; ———, uncontrolled flow; --o--, controlled flow

For the estimation of control performance, we measured the total viscous drag acting on the wall by averaging the viscous wall-shear stress over the downstream. The viscous drags in the Blasius boundary layer flow without disturbances, the uncontrolled flow, and the controlled flow are compared in Fig. 13. In the uncontrolled flow, the drag increases rapidly in the early simulation and then is getting to decrease gradually. However, after $t>300$, the drag increases slowly due to the unstable disturbances observed in Figs. 6-12. In the controlled flow, the drag undergoes the transient phenomena in the beginning of control, followed by the gradual increase. Nonetheless, it decreases down less than that of the laminar Blasius flow. In the long run, it recovers the laminar Blasius drag.

5. Conclusion

In this paper, we successfully control the transition in the Blasius boundary layer flow via the reduced-order linear controller. First, we applied the distributed reduced-order two-dimensional controller, which is designed from the linearized Navier-Stokes equations in a Poiseuille channel flow, to the linear two-dimensional boundary layer flows with two different Reynolds numbers (Re_{δ_*}=516 and 900). This controller not only works, but also is robust with respect to the Reynolds number uncertainty even in the other

basic plant than the Poiseuille flow.

Second, we applied our reduced-order controller to a two-dimensional boundary layer flow with finite amplitude disturbances at $Re_{\delta^*}=516$. We successfully suppress the nonlinear disturbances, which otherwise undergo instability, and recover the laminar Blasius boundary layer flow. A small gain in the viscous drag is obtained compared with the uncontrolled flow. Extension of H_2 to the boundary layer flow is in progress.

Acknowledgment

This work is supported by AFOSR Grant No. F49620-97-1-0276 and the computer time has been provided by the San Diego Supercomputer Center.

References

Akhavan, R., Jung, W. J. and Mangiavacchi, N., 1993, "Turbulence Control in Wall-Bounded Flows by Spanwise Oscillations," *Appl. Sci. Res.*, Vol. 51, p. 299.

Berger, T., Lee, C., Kim, J. and Lim, J., 2000, "Turbulent Boundary Layer Control Utilizing the Lorentz Force," *Phys. Fluids*, Vol. 12, No. 3, p. 631.

Bewley, T. and Liu, S., 1998, "Optimal and Robust Control and Estimation of Linear Paths to Transition," *J. Fluid Mech.*, Vol. 365, p. 305.

Bewley, T. and Moin, P., 1994, "Optimal Control of Turbulent Channel Flow," *ASME Conference*, ASME DE-Vol. 75.

Choi, H., Moin, P. and Kim, J., 1994, "Active Turbulence Control for Drag Reduction in Wall-Bounded Flows," *J. Fluid Mech.*, Vol. 262, p. 75.

Choi, H., Temam, R., Moin, P. and Kim, J., 1993, "Feedback Control for Unsteady Flow and Its Application to the Stochastic Burgers Equation," *J. Fluid Mech.*, Vol. 253, p. 509.

Cortelezzi, L. and Speyer, J. L., 1998, "Robust Reduced-Order Controller of Laminar Boundary Layer Transitions," *Phys. Rev. E*, Vol. 58, No. 2, p. 1906.

Cortelezzi, L., Lee, K. H., Kim, J. and Speyer, J. L., 1998, "Skin-Friction Drag Reduction via Robust Reduced-Order Linear Feedback Control," *Int. J. Comp. Fluid Dyn.*, Vol. 11, No. 1-2, p. 79.

Door, F. W., 1970, "The Direct Solution of the Discrete Poisson Equation on a Rectangle," *SIAM Rev.*, Vol. 12, p. 248.

Door, F. W., 1973, "Direct Methods for the Solution of Poisson's Equation on a Staggered Grid," *J. Computational Physics*, Vol. 12, p. 422.

Doyle, J. C. and Stein, G., 1981, "Multivariable Feedback Design : Concepts for a Classical/Modern Synthesis," *IEEE Trans. on Automatic Control*, AC-26(2).

Gad-el-Hak, M. and Bushnell, D. M., 1991, "Separation Control : Review," *Journal of Fluids Engineering*, Vol. 113, p. 5.

Gad-el-Hak, M., 1994, "Interactive Control of Turbulent Boundary Layer-A Futuristic Overview," *AIAA Journal*, Vol. 32, No. 9, p. 1753.

Gad-el-Hak, M., 1989, "Flow Control," *Applied Mechanics reviews*, Vol. 42, No. 10, p. 261.

Joshi, S., Speyer, J. L., and Kim, J., 1995, *Proc. 34th Conference on Decision and Control*, New Orleans, Louisiana.

Joshi, S., Speyer, J. L. and Kim, J., 1997, "A Systems Theory Approach to the Feedback Stabilization of Infinitesimal and Finite-Amplitude Disturbances in Plane Poiseuille Flow," *J. Fluid Mech.*, Vol. 332, p. 157.

Joshi, S., Speyer, J. L. and Kim, J., 1999, "Finite Dimensional Optimal Control of Poiseuille Flow," *J. Guidance, Control, and Dynamics*, Vol. 22, No. 2.

Kim, J. and Moin, P., 1985, "Application of a Fractional-Step Method to Incompressible Navier-Stokes Equations," *J. Computational Physics*, Vol. 59, p. 308.

Koumoutsakos, P., 1999, "Vorticity Flux Control for a Turbulent Channel Flow," *Phys. Fluids*, Vol. 11, No. 2, p. 248.

Laurien, E. and Kleiser, L., 1986, "Numerical Simulation of Boundary-Layer Transition and Transition Control," *J. Fluid Mech.*, Vol. 199, p. 403.

Lee, C., Kim, J., Bobcock, D. and Goodman, R., 1997, "Application of Neural Networks to

Turbulence Control for Drag Reduction," *Phys. Fluids*, Vol. 9, No.6, p. 1740.

Lee, Keun H., 1999, "A System Theory Approach to Control of Transitional and Turbulent Flows," Ph. D. dissertation, Dept. of Mechanical Eng. Univ. of California, Los Angeles, CA.

Lee, Keun H., Cortelezzi, L., Kim, J. and Speyer, J. L., 2001, "Application of Robust Reduced-Order Controller to Turbulent Flows for Drag Reduction," *Phys. Fluids*, Vol. 13, No. 5, p. 1321.

Lele, S. K., 1991, "An Improvement of Fractional Step Methods for the Incompressible Navier-Stokes Equations," *J. Computational Physics*, Vol. 92, p. 369.

Lele, S. K., 1992, "Compact Finite Difference Schemes with Spectral-like Resolution," *J. Computational Physics*, Vol. 103, p. 16.

Lim, J. and Kim, J., 2000, "A Linear Process in Wall-Bounded Turbulent Shear Flows," *Phys. Fluids*, Vol. 12, No. 8, p. 1885.

Modi, V. J., 1997, "Moving Surface Boundary-Layer Control: A Review," *Fluids and Structures*, Vol. 11, No. 6, p. 627.

Reed, H. L., Saric, W. S. and Arnal, D., 1996, "Linear Stability Theory Applied to Boundary Layers," *Annu. Rev. Fluid Mech.*, Vol. 28, p. 389.

Rhee, I. and Speyer, J. L., 1991, "A Game Theoretic Approach to a Finite Time Disturbance Attenuation Problem," *IEEE Trans., Automatic Control*, Vol. 36, No. 9, p. 1021.

Schumann, U. and Sweet, R. A., 1988, "Fast Fourier Transforms for Direct Solution of Poisson's Equation with Staggered Boundary Conditions," *J. Computational Physics*, Vol. 75, p. 123.

Zang, T. A. and Hussaini, M. Y., 1985, "Numerical Experiments on Subcritical Transition Mechanisms," *AIAA Paper*, 85-0296.

Zhou, K., Doyle, J. C. and Glover, K., 1996, Robust and Optimal Control, Prentice Hall.